NUMERICAL SIMULATIONS OF THE APOLLO S-IVB ARTIFICIAL IMPACTS ON THE MOON.

A. Rajšić[1], K. Miljković[1], T. Kawamura[2], G.S. Collins[3], N. Wójcicka[3], P. Lognonné[2], M.A.Wieczorek[4], I. J. Daubar[5]. [1]School of Earth and Planetary Sciences, Space Science and Technology Center, Curtin University, Australia (andrea.rajsic@postgrad.curtin.edu.au), [2]Institute de Physique du Globe de Paris, France, [3]Imperial College London, London, United Kingdom, [4]Observatoire de la Côte d'Azur, CNRS, Laboratoire Lagrange, France, [5]Brown University, Providence, RI, USA

Rationale: Seismic data obtained by the Apollo seismic network of the Apollo's Saturn Booster (S-IVB) drops suggested that the seismic efficiency on the Moon could be at the order of 10^{-6}-10^{-5} [1]. In this work, we recreate the same impact conditions using numerical impact shock physics code and calculate the seismic efficiency associated with these impacts. The aim is to validate the application of the code in quantification of seismic efficiency in impact events in general.

Introduction: The NASA InSight Mission has been operating on the surface of Mars since November 2018. In the first nine months of science operations, the seismometer detected 174 seismic signals [2]. However, none of these signals was unambiguously associated with an impact event [3]. See also [4] of the same issue, which discussed impact events that occurred on Mars since the InSight landing.

This calls for further investigation of meteorite strikes on planetary surfaces and the relationship between impact conditions and seismic activity. Artificial impacts made by the Apollo's Saturn boosters (S-IVB) drops [1] represent unique large-scale impact experiments (Figure 1). They provide a unique link between impact conditions and the final crater, because the impact conditions (mass and speed) were constrained. The Apollo seismic network operating on the Moon at the time recorded these impacts [1,5-6]. Therefore, these impact events can be used to validate our numerical approach for estimating seismic efficiency in the cratering process.

The Saturn S-IVB combined with the J2 engine and the instrument ring had a mass of about 14 t [1,5-6]. The booster was 6.6 m in radius and 17.8 m in length. Although it was made of aluminum, the bulk density was only 23 kg/m^3 because the structure was hollow. The impact speed at ground was 2.543 km/s [6]. The orientation of the booster (at which it was dropped from orbit) was reported to be between 13.2° and 35.0° from vertical [6]. The center of mass was located near the bottom end of the booster, likely causing a reorientation at the ground level, therefore, the exact position of the booster with respect to the surface during impact are unknown. The resulting craters formed by these artificial impacts were asymmetric with a central mound (Figure 1). The long and short axes of these craters were 34.4-38.7 and 28.6-31.9 m, respectively, and the depth was 2-3 m on average [6].

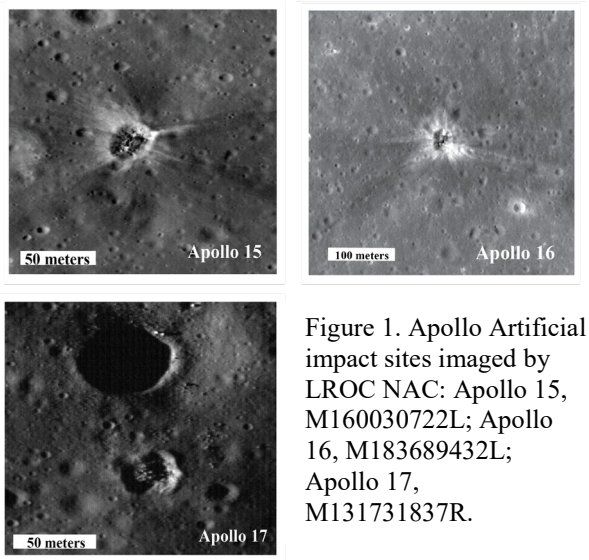

Figure 1. Apollo Artificial impact sites imaged by LROC NAC: Apollo 15, M160030722L; Apollo 16, M183689432L; Apollo 17, M131731837R.

Approach: In previous work [7-9] we used iSALE-2D shock physics code [10-12] to quantify seismic efficiency of small impacts on Mars. Using the same method in this work, we reproduced the Apollo S-IVB impacts on the Moon. We simulated both the crater formation and the pressure wave propagation.

iSALE-2D uses axial symmetry, and therefore, we needed to simplify the projection of the impactor as well as its mass distribution. We investigated five different cases of Saturn S-IVB representation, with the same mass, as the impactor at ground level. In aim to reduce density of aluminum four had 90% porosity and one was non-porous: 1) 90% porous full projected length of a hollow cylinder; 2) 90% porous half projected length of a hollow cylinder; 3) 90% porous sphere; 4) non-porous sphere; and 5) 90% porous vertical projection of the full length of the hollow cylinder. In the first two cases and the last case, we used the median value of drop angle for all S-IVB impacts (21.8° from vertical [6]) to project length to the horizontal axis (Cases 1 and 2) and to the vertical axis (Case 5), respectively. We simulated a couple of spherical cases (90% porous and non-porous) too, to investigate dependence of the cratering efficiency on the impactor shape. In all models, we maintained the mass of the booster so that the kinetic energy of the impact remained constant and realistic.

The projectile was modelled using the Tillotsen equation of state for aluminum [13]. The material strength was modelled using Johnson and Cook model

[14]. We applied ε-α porosity model [12]. The target was modeled as a 44% porous basalt for all impactor cases [7-9]. The excavation depth in these craters was approximated to be no more than 3 m [6]. Therefore, in this work, we consider a uniform target. For the target, we used the Tillotson equation of state for basalt [13] the Lundborg strength model [15], as well as ε-α porosity model [12] that we used in previous work [9].

Results:

Crater morphology. The crater formation was modelled until the transient crater formation (Figure 2). The transient crater diameter was between 21.2 and 29.2 m for all cases. To estimate the final crater size, the transient crater diameter was multiplied by 1.25 (based on simple crater scaling laws [16-17]). The transient crater depth varied with the shape of projectile, from 4.8 to 13.32 m. To estimate the final crater depth, we used similar simple crater scaling equations from [16-17]. All five cases gave different final crater depth to diameter (d/D) ratios: 0.1, 0.24, 0.25, 0.21, and 0.3, respectively for Cases 1-5. The d/D ratio for observed craters on the Moon was ~0.09. The horizontally projected impactor (Case 1) produced the final crater diameter and depth 27% and 50% smaller than in the vertical impactor case (Case 5), respectively.

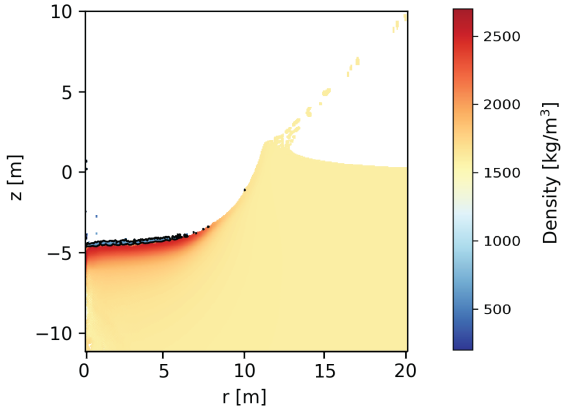

Figure 2. Density color mesh plot showing the transient crater of the best case scenario (Case 1) and the projectile residual at the bottom of the crater showing in blue (and marking its low density).

Seismic efficiency. To quantify seismic efficiency, the pressure wave needs to reach the domain in which pressure decays comparably to material strength [7-9]. Here we used the distance of 15 final crater radii (Figure 3), which should suffice based on previous works [18]. Pressure decay observed on Figure 3 shows similar decay behavior in all cases (the same impact energy, mass and speed, but different projectile size and shape). The resulting seismic efficiency was at the order of ~10^{-6}, ranging from 8.33×10^{-7} for Case 1 to 1.46×10^{-6} for Case 5. Our numerical approach is in agreement with lower estimates from [1]. Future work will address more possibilities in aim to investigate upper limits of [1].

Conclusion: This work provides two outcomes: a) The effects of the impactor shape on the final crater morphology suggested that the full projected length of the cylinder resulted in the crater morphology most similar to the once observed on the Moon (Case 1), both as crater diameter and depth. b) The seismic efficiency remained the same order magnitude for all impactor geometries, suggesting neither the impactor shape nor the impactor density have a dominant effect on the seismic efficiency estimates.

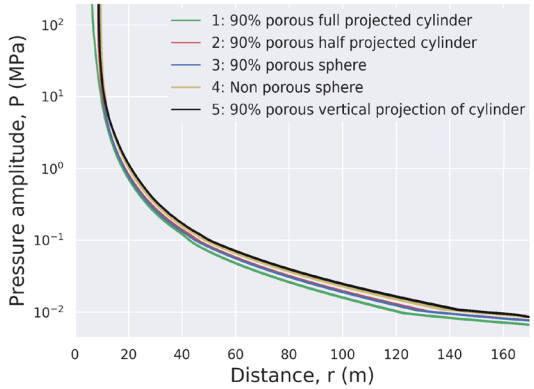

Figure 3. Pressure decay with distance for Cases 1-5. The pressure was measured radially through the target starting from the impact point.

Acknowledgments: AR and KM are fully funded by the Australian Government through the ARC (DE180100584, DP180100661). We gratefully acknowledge the developers of iSALE (https://isale-code.github.io/index.html).

References: [1] Latham G. et al. (1970) *Science* 170, 620-626. [2] Banerdt, W.B. et al. (2020) *Nature Geosci.* 13:183–189. [3] Daubar, I.J. et al. (2020) *J. Geophys. Res. Planets*, 125(8). [4] Miljković et al. (2020) *LPI (this issue)*. [5] Wagner, R., et al. (2017) *Icarus* 283, 92–103. [6] Plescia, J., et al. (2016) *Planet. Space Sci.* 124, 15–35. [7] Wójcicka, N. et al. (2020) *J. Geophys. Res. Planets,* 125(10). [8] Rajšić et al. (2020*) LPI (2326),* 1793. [9] Rajšić et al. (2020) *J. Geophys. Res. Planets, in review* [10] https://isale-code.github.io/ [11] Collins G.S. et al. (2004) *Meteorit. Planet. Sci.* 39, 217–231. [12] Wünnemann, K. et al. (2006) *Icarus* 180:514–527. [13] Tillotson, J. H. (1962) *Technical report GA-3216, General Atomic Report*. [14] Johnson G.R. & Cook W.H. (1983*) ISB Conf. Proc.* 21, 541–547. [15] Lundborg N. (1968) *Int. J. Rock Mech. Min. Sci.* 5: 427-454. [16] Grieve, R., & Garvin, J. (1984) *J. Geophys. Res. Solid Earth,* 89(B13), 11561–11572. [17] Collins G.S. et al. (2005) *Meteorit. Planet. Sci.* 40, 817-840. [18] Matsue et al. (2020) *Icarus,* 338, 113520.